Accepted Manuscript

Trimesic acid on Cu in ethanol: potential-dependent transition from 2-D adsorbate to 3-D metal-organic framework

Philipp Schäfer, Anusha Lalitha, Paula Sebastian, Santosh Kumar Meena, Juan Feliu, Marialore Sulpizi, Monique A. van der Veen, Katrin F. Domke

Please cite this article as: Philipp Schäfer, Anusha Lalitha, Paula Sebastian, Santosh Kumar Meena, Juan Feliu, Marialore Sulpizi, Monique A. van der Veen, Katrin F. Domke, Trimesic acid on Cu in ethanol: potential-dependent transition from 2-D adsorbate to 3-D metal-organic framework, *Journal of Electroanalytical Chemistry* (2017), doi: 10.1016/j.jelechem.2017.01.025

Trimesic acid on Cu in ethanol: potential-dependent transition from 2-D adsorbate to 3-D metal-organic framework

Philipp Schäfer,[a] Anusha Lalitha[b], Paula Sebastian[c], Santosh Kumar Meena[d,e], Juan Feliu[c], Marialore Sulpizi[b], Monique A. van der Veen[f]*, and Katrin F. Domke[a]*

[a]*Max Planck Institute for Polymer Research, Ackermannweg 10, 55128 Mainz, Germany Email: domke@mpip-mainz.mpg.de*
[b]*Johannes Gutenberg University, Department of Physics, Staudingerweg 7, 55128 Mainz, Germany*
[c]*Universidad de Alicante, Instituto de Electroquímica, C. Alicante S/N, 03690 San Vicente del Raspeig, Alicante, Spain*
[d]*Past address: Johannes Gutenberg University, Department of Physics, Staudingerweg 7, 55128 Mainz, Germany*
[e]*Current address: Department of Chemistry and Biochemistry, University of California, San Diego, 9500 Gilman Drive # 0314, CA La Jolla 9293*
[f]*Delft University of Technology, Faculty of Applied Sciences, Chemical Engineering Department, Section of Catalysis Engineering, Van der Maasweg 9, 2629HZ Delft, The Netherlands Email: m.a.vanderveen@tudelt.nl*

Abstract

We report the potential-dependent interactions of trimesic acid with Cu surfaces in EtOH. CV experiments and electrochemical surface-enhanced Raman spectroscopy show the presence of an adsorbed trimesic acid layer on Cu at potentials lower than 0 V vs Cu. The BTC coverage increases as the potential increases, reaching a maximum at 0 V. Based on molecular dynamics simulations, we report adsorption geometries and possible structures of the organic adlayer. We find that, depending on the crystal facet, trimesic acid adsorbs either flat or with one or two of the carboxyl groups facing the metal

surface. At higher coverages, a multi-layer forms that is composed mostly of flat-lying trimesic acid molecules. Increasing the potential beyond 0 V activates the Cu-adsorbate interface in such a way that under oxidation of Cu to Cu^{2+}, a 3-D metal-organic framework forms directly on the electrode surface.

Keywords: metal-organic frameworks, self-assembled monolayers, Cu UPD, organic electrolytes

---

1. Introduction

Organic molecules with higher order symmetry and surface-active functionalities have attracted significant attention as building units for molecular networks on all kinds of substrates.[1, 2, 3, 4] Molecule-metal interactions are of particular interest as they promise possible applications in self-assembly driven surface patterning [5, 6, 7] or electronic-state engineering of the underlying metal.[8, 9, 10] Trimesic Acid (1,3,5-benzenetricarboxylic acid, BTC) has been the poster child for the study of specific interactions between coinage metals and organic acids. The behavior of BTC, especially on single crystal Au surfaces, has been investigated with regard to changes in monolayer structure at different surface coverages [11] or different temperatures under UHV conditions.[12] At the solid-liquid interface, BTC has been investigated as building block for 2-D porous networks, for example, on highly ordered pyrolytic graphite that can host molecules in its pores.[13, 14]

BTC is also used as linker to build hybrid metal-organic frameworks (MOF) such as CuBTC (HKUST-1)[15], MoBTC (TUDMOF-1)[16] or ZnBTC.[17] Some of these structures are accessible through electrochemical synthesis

2

routes in an organic solvent through oxidation of a metal substrate in a solution of BTC.[18] CuBTC is of special interest here since it is one of the few electrochemically grown MOFs that form directly on electrode surface, as opposed to in the bulk-solution phase.[19] While some studies on BTC-metal interactions in aqueous electrolytes at different electrochemical potentials do exist,[20, 21] little is still known about the interaction of BTC with metal surfaces in organic solvents as commonly employed in MOF synthesis. Moreover, the potential-dependent metal-BTC interaction and its possible influence on the resulting framework properties, such as its adhesion or crystal orientation with respect to the surface, are unknown. Such knowledge would provide an important step toward potential-tuned growth of functional MOF materials.

The electronic structure of the metal electrode can easily be controlled through the applied potential in a standard three-electrode electrochemical setup. For coinage metals, additional vibrational spectroscopic information about the potential-dependent processes at the metal-adsorbate interface can be gathered with surface-enhanced Raman spectroscopy.[22] The combination of electrochemistry and surface-enhanced Raman spectroscopy (EC-SERS) has been extensively used to study metal-adsorbate interactions at solid/liquid interfaces.[23, 24]

We set out to investigate the potential-dependent Cu-BTC interactions in EtOH. Using Au(111) as a substrate for electrochemical investigation of Cu (underpotential-) deposition and oxidation, we performed cyclic voltammetry (CV) to observe the effect of BTC on the energetics of Cu electrochemistry in EtOH (Figure 1 a)). We complement our findings with EC-SERS experiments performed on polycrystalline Cu to obtain in-situ information about

3

the potential-dependent adsorption characteristics of BTC on Cu. Our experimental findings are expanded further by molecular dynamics simulations to gain structural information about the Cu-BTC interface. Finally, we spectroscopically observe the potential-triggered transition of BTC from a surface adsorbate into an integral building block of a 3D MOF (Figure 1 b)).
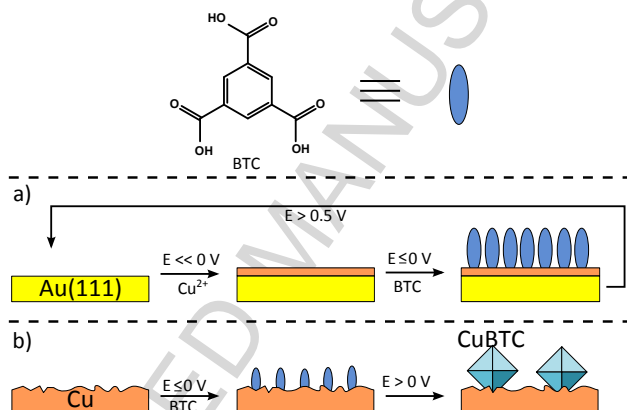

Figure 1: a) Schematic representation of the CV experiments on Au(111). Dissolved Cu ions are reduced and deposited at negative potentials and removed at positive potentials. b) Representation of the EC-SERS experiments of potential-dependent BTC-Cu interaction. Below 0 V vs Cu, adsorption of BTC takes place while above 0 V vs Cu, BTC and Cu form CuBTC MOF crystals.

2. Experimental details

2.1. Materials

EtOH (G CHROMASOLV, 99.9 %), Cu nitrate hemipentahydrate and methyltributylammonium methylsulfate ($\geq$ 95%) were received from Sigma Aldrich. BTC ($\geq$ 98%) was received from Santa Cruz Biotechnology. All chemicals were used without further purification. Polycrystalline Cu electrodes (99.99 %) were received from GAMETEC Analysentechnik. The

4

Au(111) single crystal was obtained from small single crystal beads that were oriented, cut and polished by Clavilier's method.[25, 26] The bead was produced by using a very small flame from a hand torch (propane-oxygen) to melt a Au wire and slowly cooling the melted bead.[27]

2.2. Methods

Electrochemical measurements on Au(111) were performed using a μ-Autolab III potentiostat (Eco-Chemie, Utrecht, The Netherlands) in the current-integration mode. A Cu wire polished with fine-grit polishing paper prior to immersion in the electrolyte was used as a reference electrode. Flame-annealed Au wire was used a counter electrode. All glassware was previously immersed in 40 % nitric acid over night and boiled in ultrapure water (18.8 MΩ) twice. All potentials are reported versus Cu.

The Au(111) working electrode was flame annealed before cooling in the Argon saturated atmosphere over the degassed electrolyte. Degassing was performed for at least 15 minutes. The single crystal was immersed at a potential of 0.6 V vs Cu and experiments were performed in the hanging-meniscus configuration. The supporting electrolyte was 10 g/L methyl-tributylammonium methylsulfate (MTBS) in EtOH. Experiments in Cu^{2+} ion containing solution contained 0.67 mM $Cu(NO_3)_2$ x 2.5 H_2O. If BTC was part of the electrolyte, the concentration was 75 mM. After every experiment the Au electrode was kept at a potential of 0.5 V for several minutes to remove residual Cu on the surface. The electrode was then cleaned with 40% nitric acid, copious amounts of ultrapure water and finally flame-annealed before storage.

5

Raman measurements were conducted using a home-built electrochemical Raman cell (Kel-F) designed to seamlessly exchange the electrolyte through teflon tubings. The counter- and reference-electrodes were Pt wire. The potential of the Pt-electrode used during the Raman experiments is 0.1 V vs Cu, and the potentials of the Raman experiments have been converted accordingly. The cell was cleaned in caroic acid and boiled three times with ultrapure water prior to each experiment. The Raman set-up is homebuilt with a 35 mW 633 nm HeNe cw-laser as excitation source. The spectral resolution of our setup is 1.65 cm^{-1}.[28] The maximum of the surface plasmon-resonance of Cu is located at ca. 573 nm (2.163 eV).[29] Due to the short range of the plasmon enhancement effect, the collected signal stems from the Cu-adsorbate interface and inherently makes the experiment insensitive to the bulk electrolyte.[30] Signal collection was performed in backscattering by a long working-distance air objective (Olympus LMPlan FL N, 50x, NA 0.5) parallel to the sample normal. The laser power at the sample was 2 mW. Exposure times for the spectra were 10 seconds. A full spectrum was taken every 40 seconds. All reported spectra are background-corrected with an asymmetric least-squares algorithm,[31] normalized to the C-C stretch vibration band of EtOH at 882 cm^{-1} and smoothed with a Savitzky-Golay filter. The background correction was performed in Matlab, all other data evaluation steps were performed with self-written Python code. Potential-dependent spectra are averages of 7 to 10 spectra. Time-series spectra are not averaged. Spikes from cosmic rays were removed by hand.

For the in-situ Raman measurements the polycrystalline Cu working electrode was cleaned with 25 % hydrochloric acid, rinsed with copious amounts

of ultrapure water and finally rinsed with EtOH prior to use. The electrolyte consisted of 10 g/L MTBS in 96 % EtOH / 4 % water and optionally 150 mM BTC as indicated. The cell was always first filled with pure MTBS-solution to perform a blank measurement. The electrode was afterwards kept at a constant potential of -0.4 V vs Cu while the electrolyte was exchanged to BTC containing one by hydrostatic pressure, simultaneously monitored through recording of the current. The electrolyte was flown for at least 15 minutes before the measurement in BTC containing solution was started. Raman measurements were started within 5 seconds of adjusting the potential to a new value.

3. Computational methods

3.1. Model and simulation details

We studied the adsorption of a single BTC molecule at the interface between EtOH and different Cu(100), (110) and (111) surfaces. The thickness of the Cu slab is 1.25, 0.93 and 1.1 nm for the three Cu(100), (110) and (111) surface models, respectively. The slab is solvated with an EtOH slab of 6.7 nm thickness. The details of the simulation model for the three Cu surfaces/EtOH interface with BTC molecules has been listed in Table 1, including number of atoms, molecules and box sizes. The system was charge neutral.

All molecular dynamics (MD) simulations have been performed using GROMACS package (version 5.0.2). The simulations have been performed using an atomistic force field. The force field is non-reactive and suitable to describe physisorption. Periodic boundary conditions were applied in all

7

Table 1: Model details of the Cu low index surfaces

Name of surface	No. of Cu atoms	No of BTC molecules	No of EtOH molecules	Box dimensions X, Y, Z [in nm]
Cu(100)	5000	1	2643	6.4, 6.4, 8.1
Cu(110)	3600	1	2800	6.4, 6.4, 8.1
Cu(111)	3588	1	2246	5.8, 5.9, 8.0
Cu(100)	5000	180	2040	6.4, 6.4, 8.1

three directions. The maximum force on any atom was kept smaller than 100.0 kJ/(mol·nm) for minimization of the energy after solvation. Temperature and pressure were kept constant at 300 K and 1 bar for all simulations using the Berendsen thermostat.[32] and Parrinello-Rahman coupling scheme.[33] A 2 fs time step was employed for all runs. Trajectories were saved every 30 ps. All system equilibrations were first performed using the NVT ensemble which has a constant number of particles (N), volume (V) and temperature (T) for 10 ps, and later with NPT ensemble with constant pressure (P) instead of volume. For the systems containing a single BTC molecule, the MD production runs were extended over 50 ns. Longer runs up to 500 ns were used for the higher-concentration models to obtain improved statistical sampling.

3.2. Force-field parameters

The GROMOS96 53a6 force-field package was employed for all our MD simulations.[34] Force-field parameters for BTC were generated by the Automated Topology Builder (ATB),[35] using bonded and van der Waals parameters from the GROMOS force-field. Lennard-Jones parameters for Cu metal

8

Table 2: Lennard-Jones parameters of Cu

Name of surface	C6 [kJ mol^{-1} nm^6]	C12 [10^{-5} kJ mol^{-1} nm^{12}
Cu	0.0126466271	0.20266

surfaces from Heinz et. al. [36, 37, 38], optimized to reproduce adsorption geometries and energies for organic and biomolecules at interfaces, were used and are reported in Table 2.

4. Results

4.1. CV on Au(111)

We conducted CV experiments to investigate the influence of BTC on the oxidation and reduction of Cu. As a substrate, we chose a Au(111) single-crystal surface that can be recovered during the experiments, ensuring maximal reproducibility of the results. In Figure 2, we show the CV responses of the Au(111) electrode in different electrolytes at a scan rate of 20 mV/s: The supporting electrolyte (Grey triangles) is ethanolic methyltributhylammonium methylsulfate (MTBS), a commonly used organic supporting electrolyte. The corresponding CV shows no prominent features and is governed solely by a small capacitive current in the range of -10 to 10 μA/cm^2. A lack of strong current increase towards both ends of the CV (0.7 V in anodic direction and -0.7 V in cathodic direction) shows that the electrolyte is stable in the chosen potential window.

Upon adding Cu nitrate (Cu(NO$_3$)$_2$ x 2.5 H$_2$O) to the electrolyte, the CV changes significantly (Figure 2, black line). The scan was started at 0.5 V vs Cu, a potential at which any Cu previously deposited on Au is oxidized so
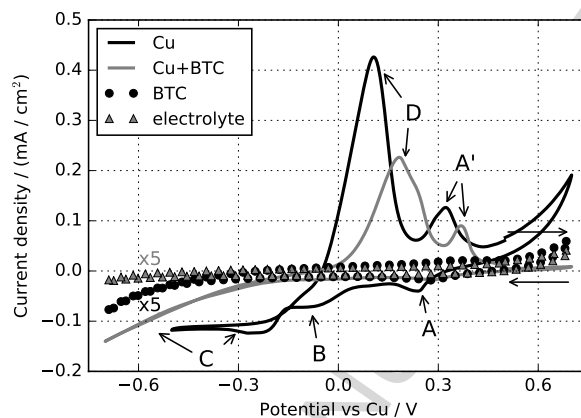
Figure 2: CV of Au(111) in supporting electrolyte with different additives. Grey triangles: pure supporting electrolyte (10 g/L MTBS in EtOH). Black line: supporting electrolyte + 0.7 mM Cu nitrate hemipentahydrate. Grey line: supporting electrolyte + 0.7 mM Cu nitrate hemipentahydrate + 75 mM BTC. Black circles: supporting electrolyte + 75 mM BTC. $v = 20$ mV/s. The current densities for the pure supporting electrolyte and for the supporting electrolyte + BTC have been multiplied by 5 for clearer display.

that the Au surface is a pristine Au(111). In the anodic direction, the current is slightly positive and shows a small increase until the scan reversal point at 0.7 V. The cathodic scan is featureless, with a slight negative slope of the current with decreasing potential till about 0.24 V where a small cathodic peak (**A**) is seen. Decreasing the potential further, a shoulder appears at -0.1 V (**B**). Below -0.15 V, the cathodic current increases slightly again, forming a small current peak at around -0.25 V. The cathodic current density slightly drops from -0.125 mA/cm^3 at the peak to -0.115 mA/cm^2 where it forms a plateau **C** till reaching the lower vertex potential of -0.5 V. After the scan reversal, the current stays constant at around -0.11 mA/cm^2 until -0.2 V where it starts increasing slowly, showing a slight hysteresis behavior in the

10

potential range from -0.2 to -0.1 V. At -0.05 V, the current increase becomes steeper (0.1 mA/cm^2 increase per 50 mV), leading to the formation of an anodic peak (**D**) at 0.11 V. At 0.32 V, a second anodic peak (**A'**) appears.

Introducing BTC into the solution leads to the CV shown as a grey line in Figure 2. Starting at a potential of 0.5 V, at a Cu-free Au(111), the anodic scan shows no features and only negligible anodic current until the first vertex potential at 0.7 V. After the scan reversal, a cathodic peak (around peak **A** for the BTC-free solution) with very low current (-17 μA/cm^2 vs the baseline of -7 μA) is detected at around 0.29 V. Scanning further, the trace stays flat and slightly negative until the cathodic current starts to increase below -0.2 V. The cathodic current increases almost linearly below -0.4 V (**C**) till the lower vertex potential of -0.7 V. The anodic scan shows a similar behavior, with a slowly decreasing cathodic current until around -0.1 V where the trace levels off. Just positive of 0 V, a large anodic peak begins (**D**) which reaches its maximum current at 0.18 V. The anodic flank of the peak shows a slight shoulder, and a second anodic peak (**A'**) appears at 0.37 V.

4.2. Electrochemical surface-enhanced Raman spectroscopy

To gain chemical insight into the interaction of BTC with the Cu surface, we performed EC-SERS on polycrystalline Cu. The experiments were performed in the potential region from -0.4 V to +0.1 V vs Cu, the area in which we see the strongest differences in the CV experiments between BTC containing and BTC-free solutions.

Figure 3 a) shows an overview of SER spectra taken at different potentials in BTC containing electrolyte. For comparison, Figure 3 b) shows the spectrum of Cu in the BTC-free supporting electrolyte MTBS in EtOH at
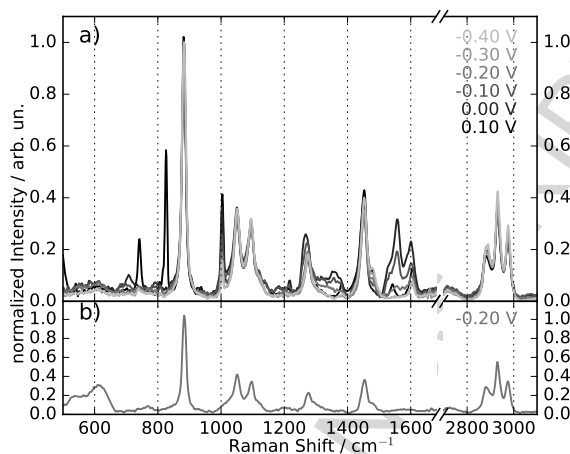
11

Figure 3: a) SER spectra of polycrystalline Cu in 75 mM BTC + 10 g/L MTBS in EtOH with increasing potential (bright to dark). b) SER spectrum of polycrystalline Cu in 10 g/L MTBS in EtOH at -0.2 V. All spectra are normalized to the C-C stretch mode of ethanol at 882 cm^{-1}.

-0.2 V. The spectrum of the supporting electrolyte does not change with the applied potential in the chosen potential region between -0.4 and 0.1 V.

We will first generally describe the spectral regions that change with applied potential and then discuss specific bands in detail (Figures 4,5). There are four areas in the spectrum that show changes in the SER response upon BTC addition to the supporting electrolyte. Between 500 and 650 cm^{-1}, we observe two broad peaks in Figure 3 b) that are absent in the corresponding spectrum in Figure 3 a). Upon addition of BTC, these bands disappear and do not reappear at any potential under our chosen experimental conditions. The second area of interest lies between 725 and 850 cm^{-1}. Here, we observe two bands with high intensity in BTC containing solution at 0.1 V. These bands are undetectable in any spectra between -0.3 V and 0 V and only appear in BTC-containing solution. In the third area of interest between 1530
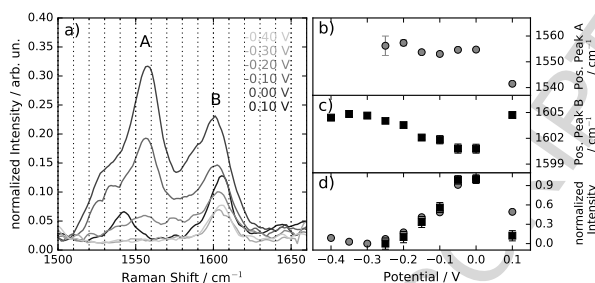
12

Figure 4: a) Zoom of the SER spectra in the area from 1500 to 1660 cm^{-1} at different potentials. Right: Results of a Lorentzian fit of the area from 1500 to 1660 cm^{-1}: **b)** & **c)** fitted peak maximum position of peaks A and B, respectively, as a function of potential. **d)** maximum peak intensity of peaks A (grey, circles) and B (grey, squares) relative to the respective peak's maximum observed intensity in the given potential window. Peaks B in the SER spectra at -0.4 V, -0.35 V and -0.3 V were fitted with a single Lorentzian since peak A is absent in these spectra. Error bars are errors of the fits.

and 1610 cm^{-1}, we observe new bands at all investigated potentials that are not present in the spectrum of the pure supporting electrolyte. Lastly, at 1002 cm^{-1} we observe a new band in the presence of BTC. The intensity of this band increases with more positive potentials. The changes in the area from 1300 to 1400 cm^{-1} are artifacts of the background removal during data processing. We will now first focus on the area between 1500 and 1650 cm^{-1} and describe the potential-dependent changes in the peak structure in depth.

Figure 4 a) shows a zoom of the EC-SER spectra obtained at different potentials in the region from 1500 cm^{-1} to 1670 cm^{-1}. The spectra show two distinct peaks, one around 1560 cm^{-1} (peak A) that cannot be detected at all potentials, and one around 1605 cm^{-1} (peak B) present in varying intensity at all investigated potentials. The right side of Figure 4 shows the peak positions and maximum peak intensities obtained from fitting the bands

13

with two Lorentzian profiles. Figure 4 b) and c) show the positions of peak A and B, respectively. Figure 4 d) shows the maximum peak intensities of both peaks normalized to their respective maximum intensities in the measured potential window. We observe that peak A cannot be distinguished from the noise at potentials below -0.25 V. The position of peak A shows slight variations between 1555 and 1553 cm^{-1} in the range from -0.25 V to 0 V. After crossing the 0 V threshold, the peak red-shifts to 1541 cm^{-1} at 0.1 V. The general trend of the shift is opposite for peak B. The peak position starts at 1605 cm^{-1} at -0.4 V and gradually red-shifts to 1601 cm^{-1} at 0.0 V. After crossing the threshold, it blue-shifts back to 1605 cm^{-1} at 0.1 V. The shifts of the two peaks span a range of 14 and 4 cm^{-1} for peak A and B, respectively, meaning that the position of peak A is more strongly affected by the applied potential.

The change in peak intensity with varying potential shows the same trend for both peaks. While peak A can only be distinguished above -0.3 V, both peaks rise monotonously in intensity and reach their maximum intensities at 0 V. At 0.1 V, the peak intensities are significantly lower. The increase of the peak intensity at more positive potentials is reversible in the sense that changing the potential from -0.2 V to -0.1 V and back shows a reversible increase and decrease in the signal (data not shown). We observe that for high intensities (-0.1 V and 0 V in Figure 4, left), peak A has a shoulder around 1530 cm^-1. We will discuss the presence of this shoulder later since for most spectra, the shoulder cannot be distinguished from the noise. The spectra below 0 V and at 0.1 V are stable over the time frame of the experiment (5 minutes). We do not show the fit results of an average spectrum at 0.05 V
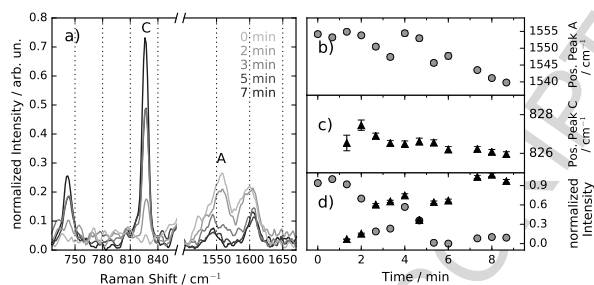
14

Figure 5: a) Zoom of the SER spectra in the areas from 725 to 860 cm^{-1} and from 1500 to 1670 cm^{-1} at different times after switching the potential to 0.05 V. Darker spectra were taken at later times after the potential step. Right: fit results for peaks A and C. **b)** & **c)** Fitted peak-maximum position of peaks A and C, respectively, at different times. **d)** Fitted maximum peak intensities of peaks A (grey, circles) and C (triangles, black), normalized to the respective peak's maximum observed intensity in the experimental timeframe. Error bars are errors of the fits.

here since the SERS response shows large changes over time which we will describe in detail below.

While Figure 4 shows a significant change in the SERS response of BTC/Cu after crossing a potential of 0 V, we now want to further investigate what happens just above 0 V. Figure 5 a) shows the Raman signal evolving over time at 0.05 V both in the previously explored area from 1550 to 1670 cm^{-1} as well as in the spectral region from 725 to 860 cm^{-1}. A spectrum was taken every 40 seconds. For clarity, only a selected number of spectra are shown in the overview on the left. We can see that in the area from 725 to 860 cm^{-1}, two peaks appear after 2 minutes and increase in intensity throughout the experiment. Meanwhile in the higher wavenumber region, the previously described peaks A and B change considerably.

Figure 5 b) shows the frequency shift of peak A in detail over time. The

15

position of peak A shifts from 1555 cm^{-1} to 1540 cm^{-1} over the 10-minute time period. The intensity of peak A (Figure 5 d), grey circles) shows a slow decrease over time. The observed frequency shifts and intensity changes of peak A reflect the transition from the previously discussed spectrum at 0 V to the final spectrum at 0.1 V (Figure 4). Figure 5 c) displays the time-dependent position of peak C whose changes are within 1 cm^{-1}. The intensity of peak C (Figure 5 d), black triangles) increases at a similar rate as the intensity of peak A decreases. In the beginning, peak C is not distinguishable from the noise, and only starts being visible after 80 seconds. The intensity increases with time, albeit not monotonously. After 7 minutes, the intensity stabilizes and shows no significant changes over the last 2 minutes of the experiment. In fact, the whole spectrum shows only small changes throughout the last two minutes of the experiment.

4.3. Molecular dynamics simulations

To gain insight into the adsorption geometry and surface structure of BTC on Cu in EtOH, we performed MD simulations on the adsorption of BTC on the most stable low index Cu surfaces, namely (100), (110) and (111). The idea is to provide an atomistic description of the liquid structure at the solid/electrolyte interface, taking into account both, temperature effects and the explicit treatment of the solvent. MD simulations were carried out at room temperature (300 K) and explicitly including a BTC/EtOH solution.

An overview of different binding configurations of a single BTC molecule on Cu is reported in Figure 6. The configurations reported represent minima in the energy surface in the presence of explicit (ethanol) solvent. On all the three surfaces, BTC favorably binds to the Cu surface, however the
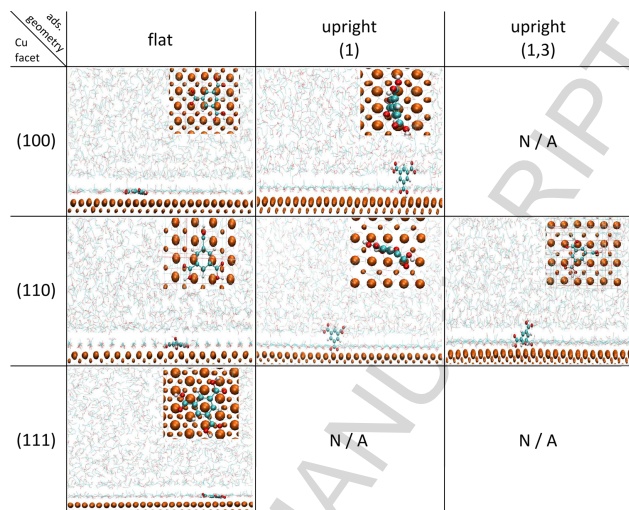
16

Figure 6: Adsorption snapshots for a single BTC molecule on low-index Cu surfaces for different adsorption geometries taken from MD simulations.

binding configurations and adsorption energies depend on the surface plane. In particular, on Cu(111), adsorption in the flat configurations is the most favorable. On Cu(100), flat and upright configurations have a similar binding affinity, while on Cu(110) flat, upright and two legged upright configurations are possible. The binding energies for all investigated cases are reported in Table SI 1.

Increasing the concentration of BTC in the simulation box allows us to investigate the ensemble structures that form when more BTC adsorbs on the Cu(100) surface. In particular, here we discuss the case of a Cu(100) surface in contact with a 1.12 M BTC in EtOH (bulk) solution, which corresponds to 180 BTC molecules in the simulation box. Note that the actual interface concentration can be higher, given the high propensity of BTC to adsorb on the Cu surfaces. In Figure 7, a snapshot of the Cu/electrolyte interface from
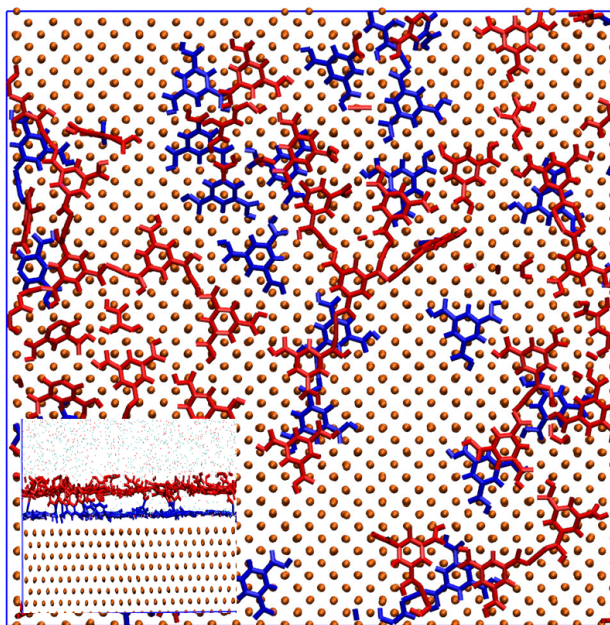
17

Figure 7: Adsorption structure on Cu(100) for a simulation containing 180 BTC molecules in the EtOH phase. The inset shows a side view of the same structure. Blue and red are the first and second layer of H3BTC molecules respectively starting from the Cu surface.

the MD trajectory is reported.

The first adsorbed layer on the Cu(100) surface is formed by both EtOH and BTC molecules. This can be observed from the density profile reported in Figure SI 3. 41% of the BTC molecules in this first layer adsorb flat on the surface, with the molecular plane forming an angle smaller than 10 degrees with the surface plane. 32% of the molecules are found instead in a standing upright configuration, with the molecular plane forming an angle larger than 30 degrees with respect to surface plane. Interestingly, a second well-structured layer of molecules is also observed. In this second layer, most of the BTC molecules (60%) are found in flat configuration as

18

well, with their molecular plane parallel to the Cu(100) plane. These BTC molecules can interact either directly with the BTC molecules in the first adsorbed layer or with the highly ordered layer of EtOH. Along the z direction (direction normal to the surface), BTC and EtOH molecules are perfectly commensurate, which favors the formation of a well-ordered layer at the interface. Note the coinciding peak positions for BTC and EtOH density along the z-direction in Figure SI 3.

5. Discussion

5.1. Potential-dependent adsorption behavior of BTC on Cu

Features **B** and **C** in the CVs of Cu nitrate in EtOH (Figure 2, black line) concern the reduction of Cu and subsequent deposition on the Au surface, with the shoulder **B** possibly being a prereduction of Cu^{2+} to Cu^+. Peak **D** corresponds to the oxidation of this Cu layer on the electrode (most likely to Cu^{2+}). The peak-pair **A** and **A'** are the anodic and cathodic sides of the same reaction, since peak **A'** is absent in experiments that do not scan below 0.3 V. Both features are also absent in experiments without Cu as evident from the comparison with the CV in pure electrolyte (Figure 2, grey triangles). It is therefore reasonable to conclude that the peaks belong to an underpotential deposition (UPD) process of Cu on the Au electrode, similar to what is observed in aqueous Cu salt solutions.[39] An observed deposition potential of 0.24 V vs Cu closely matches the potential of 0.21 V vs Cu/Cu^{2+} previously observed in aqueous sulfuric acid solution.[40] It should be noted that even after multiple scans, the first CV can be reproduced, meaning that the Au(111) surface is free of residual Cu above 0.4 V. If Cu remained on

19

the surface, we would expect changes in subsequent CVs.

The CV features described after introducing BTC into the solution (Figure 2, grey line) are similar to the ones that we observe in the solution that does not contain BTC. Noteworthy is the absence of the shoulder **B** and the changes in the deposition peak A of the Cu UPD at **A**. The small peak observed around 0.3 V in cathodic scan direction where we expect to see the deposition of the Cu UPD is also observed (albeit with lower current density) in solutions containing only BTC and no Cu (Figure 2, black circles). The peak observed at 0.3 V could therefore either be the Cu UPD peak, a peak from BTC (or an impurity in the BTC) or a combination of both. The features **C**, **D** and **A'** are assigned to the same phenomena as in BTC-free solution, namely Cu bulk deposition, Cu bulk oxidation and the stripping of the Cu UPD layer.

The comparison of the CVs recorded in presence and absence of BTC reveals differences in the positions of peaks and their general shape. First, the two peaks (**D**, **A'**) are shifted towards more positive potentials and peak at lower current densities. The assigned UPD stripping peak **A'** is found 48 mV higher in the BTC containing case while the Cu oxidation peak **D** is shifted by +75 mV. The current corresponding to Cu deposition (**C**) increases much more slowly in the presence of BTC and the marked plateau features of the BTC-free CV are missing.

The presence of BTC causes an overpotential for both the deposition of Cu, as indicated by the slower and delayed rise of the cathodic currents at negative potentials, and the corresponding Cu oxidation, as evident by the shift of peak **D** to more anodic potentials. The lower currents in all

20

oxidation peaks can be explained by the lower amount of deposited Cu (due to the lower deposition currents). Likely, the induced overpotential stems from an adsorption of BTC on the Cu surface at potentials lower than 0 V. Adsorption of BTC to the surface below 0 V would explain the delayed and slowed down deposition of Cu, since Cu electrodeposition is known to be diffusion-limited[41] and BTC would act as a diffusion barrier for Cu^{2+} ions, effectively shielding the electrode from the deposition. In addition, after Cu has been deposited, BTC can adsorb onto the Cu layer, stabilizing the surface and therefore energetically hindering Cu oxidation. The shift in the UPD stripping peak **A'** can also be explained through Cu-BTC interactions, assuming that at least part of the BTC is deprotonated upon adsorption. It has been shown that anions that strongly interact with Cu^{2+} ions and Cu can shift the CuUPD process to higher potentials.[42] The possible absence of the UPD reduction peak **A** could be explained by an adsorption of BTC to the Au surface at positive potentials, as has previously been reported for the Au-aqueous electrolyte interface.[21]

The potential-dependent EC-SER spectra in Figure 3 confirm our hypothesis of adsorbed BTC on the electrode surface. Peaks A and B are assigned to the symmetric $C\text{-}O_2$ stretch vibration and C-C ring vibrations of BTC, respectively.[43] The increase in the band intensities of peaks A and B reflects an increase in the amount of BTC at the electrode at more anodic potentials. The peak at 1002 cm^{-1}, which is assigned to the ring breathing motion of BTC,[20] shows the same behavior as the 1550 and 1604 cm^{-1} bands with increasing intensity at higher potentials (data not shown in detail). From the observed increase in Raman band intensities between 1500

21

and 1610 cm^{-1} with higher potentials, we conclude that more BTC adsorbs on the Cu surface at more positive potentials. Our observation of an increase in the surface coverage of BTC at more positive potentials matches previous reports for the Au(111)-electrolyte interface. In aqueous solution, BTC switches from being physisorbed to Au at lower potentials to being chemisorbed at higher potentials.[44] This change coincides with a gradual increase in the surface coverage of adsorbed BTC at more positive potentials. In our system, according to the EC-SERS data, the BTC surface coverage is highest in the potential range from -0.05 V to 0 V. Comparing these potentials of maximum BTC coverage to the steep increase in anodic current in the CVs, we see that in BTC-free solution at -0.05 V, Cu oxidation already starts. More importantly, in BTC-free solution, there does not seem to be a potential at which neither oxidation nor deposition of Cu take place. The current trace goes from a slightly decreasing cathodic current just below -0.05 V to a quickly increasing anodic current without a period of low electrochemical activity. In BTC containing solution, however, the change in anodic current is more gradual and the current trace is almost flat around -0.05 V. Only after crossing 0 V, we observe a significant increase in the slope of the current trace. This coincides with the potential range of maximum BTC coverage as observed with EC-SERS at -0.05 and 0 V. We thus conclude that the adsorbed BTC stabilizes the surface and induces an overpotential for Cu oxidation. This is, to our knowledge, the first time that the adsorption of BTC on Cu has been shown in organic solution. To complement our experimental findings, we use MD simulations to gather detailed structural information about the BTC adlayer formation on Cu.

22

5.2. Adlayer structure from molecular dynamics simulations

The MD simulations reveal multiple possible adsorption geometries of BTC on Cu in EtOH (Figure 6). So far most of the research has concentrated on UHV conditions.[11, 12] In such conditions, BTC is known to assemble in diverse supramolecular structures due to the trigonal exodentate functionality, and the most common motif identified therein is a planar honeycomb network structure formed through the dimerization of the carboxyl groups. On Cu(100) at low temperatures ($\leq$ 280 K), flat-lying BTC molecules form islands where the honeycomb motif prevails. As the temperature increases (300 K), stripe-shaped supramolecular structures are formed.[45] This change is associated with a deprotonation of the BTC molecules, leading to carboxylate formation and an upright bonding geometry. These results demonstrate how adsorbate-substrate interactions can be exploited to drive the transformation of supramolecular arrangements at surfaces.

The presence of the solvent changes this described picture since the solvent can strongly interact with BTC through, for example, hydrogen bonds. We find that depending on the exposed crystal facet, BTC can either lie flat on the surface, or stand upright with one or two of the carboxyl groups directly binding to the surface. These multiple possible adsorption geometries yield an explanation for the SER spectral shoulder we see towards the lower energy side of the $v_{asym}CO_2$ peak at 1550 cm^{-1} (Figure 4 a)). Different adsorption geometries will give different SERS responses. The vibrations that are expected to be most affected are the ones involving the coordinating atoms, in this case the carboxyl group. A change in adsorption geometry has been observed for BTC at the Au(111)-aqueous electrolyte interface where

the structure of the BTC adlayer changes with the applied potential.[21] The molecules 'stand up' as their surface coverage increases with increasing potentials. Both flat as well as upright configurations are found in the MD simulations. The structures obtained in our study can be used as starting point for more elaborate calculations, also including the electronic structure e.g. at the Density Functional Theory level. Currently, we cannot directly link the SER spectra to the MD simulation results and thus we cannot comment on possible adsorption-geometry changes with the applied potential in our experiments. Calculations of SER spectra from the MD simulation snapshots and their detailed comparison to experiment are underway in our laboratory.

5.3. Potential-triggered transformation of the BTC adlayer to CuBTC MOF

The EC-SERS response (Figure 5) allows us to follow the potential-triggered transformation of the BTC adlayer into a crystalline 3D MOF structure in situ. Increasing the potential apparently activates the BTC/Cu interface to form a new hybrid (MOF) structure where the metal ion-molecule complex is the elemental building unit as identified by the bands at 740 and 826 cm^{-1} assigned to characteristic C-H stretch vibrations of CuBTC MOF.[43, 46]. The similar rates in band intensity decrease at 1550 cm^{-1} (adsorbed BTC) and increase at 826 cm^{-1} (BTC in CuBTC MOF) indicate that the MOF is formed at roughly the same rate as the adsorbed BTC is consumed. After 10 minutes reaction time at 0.05 V, peaks A and B perfectly reflect the Raman response of pure CuBTC.[47] The red-shift of the v_{asym}C-O$_2$ band during the synthesis of CuBTC can be explained through the influence that coordinated Cu atoms and/or ions have on the C-O$_2$ bond

strength. As in the Cu in CuBTC is in oxidation state $+2$, the coordination of BTC to Cu ions pulls electron density out of the C-O$_2$ bonds. On the Cu electrode surface, BTC coordinates to metallic Cu(0) where the electron pull is much weaker.

It should be noted that we do not detect the SER signature of Cu$_2$O in BTC containing solution. We observe the broad 515 and 615 cm^{-1} bands of Cu$_2$O in the BTC-free supporting electrolyte (Figure 2 b)), but upon flushing the cell with BTC containing electrolyte, the Cu$_2$O signature disappears. Likely, the slightly acidic linker helps to dissolve the Cu$_2$O, forming either Cu or Cu^{2+} depending on the applied potential, and water. Previously we have shown that Cu$_2$O is a necessary intermediate in the electrochemical synthesis of CuBTC.[47] The new findings presented here suggest that the Cu$_2$O intermediate is very short lived in the presence of BTC.

While the electrochemical synthesis of CuBTC MOF in EtOH has been described before,[48] this is to our knowledge the first time spectroscopic insight into the electrochemical interface during the synthesis is presented. Additionally, for the first time, a BTC-metal interaction prior to the oxidation of Cu is reported for this system. The adsorption of BTC at Cu prior to MOF formation could be the explanation for the commonly observed strong adhesion of MOF to the Cu electrode, a fairly unique property of electrosynthesized CuBTC compared to other electrochemically produced MOFs.[19] Identifying metal-linker combinations where a strong adsorption of the linker to the surface of the metal is to be expected could prove to be a valuable starting point in the ongoing search for new, surface-anchored electrosynthesized MOFs.

6. Conclusion

The potential-dependent interaction of BTC with Cu in EtOH has been investigated. CV shows an energetic delay of Cu oxidation in the presence of BTC, suggesting the formation of a molecular adlayer of BTC at the metal surface. EC-SERS confirms the existence of adsorbed BTC on Cu below 0 V vs Cu. The surface coverage of the adsorbed BTC layer is dependent on the applied potential where more cathodic potentials lead to a higher amount of adsorbed BTC. Using MD simulations, we could unveil three different possible adsorption geometries of single BTC molecules on Cu, namely flat, upright with one coordinated carboxyl group and upright with two coordinated carboxyl groups, depending on the exposed Cu basal plane. At high BTC concentration, the MD simulations predict a multi-layered structure of BTC on the surface with both flat as well as upright molecules present. Above 0 V, we observe a slow transformation within ten minutes of BTC adsorbed at metallic Cu(O) to complexed BTC-Cu(2+) in form of CuBTC MOF.

[1] M. A. Lingenfelder, H. Spillmann, A. Dmitriev, S. Stepanow, N. Lin, J. V. Barth, K. Kern, Towards Surface-Supported Supramolecular Architectures: Tailored Coordination Assembly of 1,4-Benzenedicarboxylate and Fe on Cu(100), Chemistry - A European Journal 10 (8) (2004) 1913–1919. doi:10.1002/chem.200305589. URL http://doi.wiley.com/10.1002/chem.200305589

[2] Y. Yang, C. Wang, Solvent effects on two-dimensional molecular self-assemblies investigated by using scanning tunneling microscopy, Current Opinion in Colloid & Interface Science 14 (2) (2009) 135–147. doi:10.1016/j.cocis.2008.10.002.

[3] L. Grill, M. Dyer, L. Lafferentz, M. Persson, M. V. Peters, S. Hecht, Nano-architectures by covalent assembly of molecular building blocks, Nat Nano 2 (11) (2007) 687–691. doi:10.1038/nnano.2007.346. URL http://dx.doi.org/10.1038/nnano.2007.346

[4] J. V. Barth, J. Weckesser, N. Lin, A. Dmitriev, K. Kern, Supramolecular architectures and nanostructures at metal surfaces, Appl. Phys. A 76 (5) (2003) 645–652. doi:10.1007/s00339-002-2003-6. URL http://dx.doi.org/10.1007/s00339-002-2003-6

[5] J. Liu, T. Chen, X. Deng, D. Wang, J. Pei, L.-J. Wan, Chiral Hierarchical Molecular Nanostructures on Two-Dimensional Surface by Controllable Trinary Self-Assembly, Journal of the American Chemical Society 133 (51) (2011) 21010–21015. doi:10.1021/ja209469d. URL http://pubs.acs.org/doi/abs/10.1021/ja209469d

[6] R. Decker, U. Schlickum, F. Klappenberger, G. Zoppellaro, S. Klyatskaya, M. Ruben, J. V. Barth, H. Brune, Using metal-organic templates to steer the growth of Fe and Co nanoclusters, Applied Physics Letters 93 (24) (2008) 243102. doi:10.1063/1.3040328.
URL http://dx.doi.org/10.1063/1.3040328

[7] M. Lackinger, W. M. Heckl, Carboxylic Acids: Versatile Building Blocks and Mediators for Two-Dimensional Supramolecular Self-Assembly, Langmuir 25 (19) (2009) 11307–11321. doi:10.1021/la900785f.
URL http://pubs.acs.org/doi/abs/10.1021/la900785f

[8] F. Klappenberger, D. Kuhne, W. Krenner, I. Silanes, A. Arnau, F. J. Garcia de Abajo, S. Klyatskaya, M. Ruben, J. V. Barth, Dichotomous Array of Chiral Quantum Corrals by a Self-Assembled Nanoporous Kagome Network, Nano Letters 9 (10) (2009) 3509–3514. doi:10.1021/nl901700b.
URL http://pubs.acs.org/doi/abs/10.1021/nl901700b

[9] J. Lobo-Checa, M. Matena, K. Müller, J. H. Dil, F. Meier, L. H. Gade, T. A. Jung, M. Stöhr, Band Formation from Coupled Quantum Dots Formed by a Nanoporous Network on a Copper Surface, Science 325 (5938) (2009) 300–303. doi:10.1126/science.1175141.
URL http://dx.doi.org/10.1126/science.1175141

[10] V. Iancu, K.-F. Braun, K. Schouteden, C. Van Haesendonck, Probing the Electronic Properties of Trimesic Acid Nanoporous Networks on Au(111), Langmuir 29 (37) (2013) 11593–11599. doi:10.1021/la402282x.
URL http://pubs.acs.org/doi/abs/10.1021/la402282x

28

[11] Y. Ye, W. Sun, Y. Wang, X. Shao, X. Xu, F. Cheng, J. Li, K. Wu, A Unified Model: Self-Assembly of Trimesic Acid on Gold, Journal of Physical Chemistry C 111 (28) (2007) 10138–10141. doi:10.1021/jp072726o.
URL http://dx.doi.org/10.1021/jp072726o

[12] T. Classen, M. Lingenfelder, Y. Wang, R. Chopra, C. Virojanadara, U. Starke, G. Costantini, G. Fratesi, S. Fabris, S. de Gironcoli, S. Baroni, S. Haq, R. Raval, K. Kern, Hydrogen and Coordination Bonding Supramolecular Structures of Trimesic Acid on Cu(110) , The Journal of Physical Chemistry A 111 (49) (2007) 12589–12603. doi:10.1021/jp076037o.
URL http://pubs.acs.org/doi/abs/10.1021/jp076037o

[13] G. Eder, S. Kloft, N. Martsinovich, K. Mahata, M. Schmittel, W. M. Heckl, M. Lackinger, Incorporation dynamics of molecular guests into two-dimensional supramolecular host networks at the liquid-solid interface, Langmuir 27 (22) (2011) 13563–13571. doi:10.1021/la203054k.
URL http://dx.doi.org/10.1021/la203054k

[14] S. Griessl, M. Lackinger, M. Edelwirth, M. Hietschold, W. M. Heckl, Self-assembled two-dimensional molecular host-guest architectures from trimesic acid, Single Molecules 3 (1) (2002) 25–31. doi:10.1002/1438-5171(200204)3:1¡25::AID-SIMO25¿3.0.CO;2-K.

[15] S. S. Y. Chui, S. M. F. Lo, J. P. H. Charmant, a. G. Orpen, I. D. Williams, A Chemically Functionalizable Nanoporous Material [Cu_3(TMA)_2(H_2O)_3]_n, Science 283 (February) (1999) 1148–1150.

doi:10.1126/science.283.5405.1148.

URL http://www.jstor.org/stable/2896750

[16] M. Kramer, U. Schwarz, S. Kaskel, Synthesis and properties of the metal-organic framework Mo3(BTC)2 (TUDMOF-1), Journal of Materials Chemistry 16 (23) (2006) 2245–2248. doi:10.1039/b601811d.
URL http://pubs.rsc.org/en/content/articlehtml/2006/jm/b601811d

[17] M. Eddaoudi, H. Li, O. Yaghi, Highly Porous and Stable MetalOrganic Frameworks: Structure Design and Sorption Properties, Journal of the American Chemical Society 122 (7) (2000) 1391–1397. doi:10.1021/JA9933386.
URL http://dx.doi.org/10.1021/JA9933386

[18] H. Al-Kutubi, J. Gascon, E. J. R. Sudhölter, L. Rassaei, Electrosynthesis of Metal-Organic Frameworks: Challenges and Opportunities, ChemElectroChem 2 (4) (2015) 462–474. doi:10.1002/celc.201402429.
URL http://doi.wiley.com/10.1002/celc.201402429

[19] A. Martinez Joaristi, J. Juan-Alcañiz, P. Serra-Crespo, F. Kapteijn, J. Gascon, Electrochemical Synthesis of Some Archetypical Zn 2+ , Cu 2+ , and Al 3+ Metal Organic Frameworks, Crystal Growth & Design 12 (7) (2012) 3489–3498. doi:10.1021/cg300552w.
URL http://pubs.acs.org/doi/abs/10.1021/cg300552w

[20] Y. Kim, K. Cho, K. Lee, J. Choo, M.-s. Gong, S.-W. Joo, Electric field-induced adsorption change of 1,3,5-benzenetricarboxylic acid on gold, silver, and copper electrode surfaces investigated by surface-enhanced

Raman scattering, Journal of Molecular Structure 878 (1-3) (2008) 155–161. doi:10.1016/j.molstruc.2007.08.002.
URL http://dx.doi.org/10.1016/j.molstruc.2007.08.002

[21] B. Han, Z. Li, S. Pronkin, T. Wandlowski, In situ ATR-SEIRAS study of adsorption and phase formation of trimesic acid on Au(111-25 nm) film electrodes, Canadian Journal of Chemistry 82 (10) (2004) 1481–1494. doi:10.1139/v04-118.
URL http://www.nrcresearchpress.com/doi/abs/10.1139/v04-118

[22] P. L. Stiles, J. A. Dieringer, N. C. Shah, R. P. Van Duyne, Surface-Enhanced Raman Spectroscopy, Annual Review of Analytical Chemistry 1 (1) (2008) 601–626. doi:10.1146/annurev.anchem.1.031207.112814.
URL http://dx.doi.org/10.1146/annurev.anchem.1.031207.112814

[23] Z.-Q. Tian, B. Ren, Adsorption and reaction at electrochemical interfaces as probed by surface-enhanced Raman spectroscopy, Annual Review of Physical Chemistry 55 (1) (2004) 197–229. doi:10.1146/annurev.physchem.54.011002.103833.
URL http://dx.doi.org/10.1146/annurev.physchem.54.011002.103833

[24] D.-Y. Wu, J.-F. Li, B. Ren, Z.-Q. Tian, Electrochemical surface-enhanced Raman spectroscopy of nanostructures., Chemical Society reviews 37 (5) (2008) 1025–1041. doi:10.1039/b707872m.
URL http://pubs.rsc.org/en/Content/ArticleHTML/2008/CS/B707872M

[25] C. Korzeniewski, V. Climent, J. M. Feliu, Electrochemistry at Platinum

Single Crystal Electrodes, in: Electroanalytical Chemistry. A series of Advances, CRC Press, 2011, pp. 75–170.

[26] J. Clavilier, D. Armand, S. Sun, M. Petit, Electrochemical adsorption behaviour of platinum stepped surfaces in sulphuric acid solutions, Journal of Electroanalytical Chemistry and Interfacial Electrochemistry 205 (1) (1986) 267–277. doi:10.1016/0022-0728(86)90237-8.
URL http://dx.doi.org/10.1016/0022-0728(86)90237-8

[27] A. Rodes, E. Herrero, J. M. Feliu, A. Aldaz, Structure sensitivity of irreversibly adsorbed tin on gold single-crystal electrodes in acid media, Journal of the Chemical Society, Faraday Transactions 92 (20) (1996) 3769–3776. doi:10.1039/ft9969203769.
URL http://dx.doi.org/10.1039/ft9969203769

[28] K. Stadelmann, A. Elizabeth, N. Martín Sabanés, K. F. Domke, The SERS signature of PbS quantum dot oxidation, Vibrational Spectroscopydoi:10.1016/j.vibspec.2016.08.008.
URL http://dx.doi.org/10.1016/j.vibspec.2016.08.008

[29] P. F. Robusto, R. Braunstein, Optical measurements of the surface plasmon of copper, Physica Status Solidi (b) 107 (2) (1981) 443–449. doi:10.1002/pssb.2221070207.
URL http://doi.wiley.com/10.1002/pssb.2221070207

[30] M. D. Sonntag, J. M. Klingsporn, A. B. Zrimsek, B. Sharma, L. K. Ruvuna, R. P. Van Duyne, Molecular plasmonics for nanoscale spectroscopy, Chem. Soc. Rev. 43 (4) (2014) 1230–1247.

doi:10.1039/C3CS60187K.

URL http://xlink.rsc.org/?DOI=C3CS60187K

[31] P. H. C. Eilers, A Perfect Smoother, Analytical Chemistry 75 (14) (2003) 3631–3636. doi:10.1021/AC034173T.

URL http://dx.doi.org/10.1021/AC034173T

[32] H. J. C. Berendsen, J. P. M. Postma, W. F. van Gunsteren, A. Di-Nola, J. R. Haak, Molecular dynamics with coupling to an external bath, The Journal of Chemical Physics 81 (8) (1984) 3684–3690. doi:10.1063/1.448118.

URL http://dx.doi.org/10.1063/1.448118

[33] M. Parrinello, A. Rahman, Polymorphic transitions in single crystals: A new molecular dynamics method, Journal of Applied Physics 52 (12) (1981) 7182. doi:10.1063/1.328693.

URL http://dx.doi.org/10.1063/1.328693

[34] C. Oostenbrink, A. Villa, A. E. Mark, W. F. Van Gunsteren, A biomolecular force field based on the free enthalpy of hydration and solvation: The GROMOS force-field parameter sets 53A5 and 53A6, Journal of Computational Chemistry 25 (13) (2004) 1656–1676. doi:10.1002/jcc.20090.

URL http://doi.wiley.com/10.1002/jcc.20090

[35] K. B. Koziara, M. Stroet, A. K. Malde, A. E. Mark, Testing and valida-tion of the Automated Topology Builder (ATB) version 2.0: prediction of hydration free enthalpies, Journal of Computer-Aided Molecular De-

sign 28 (3) (2014) 221–233. doi:10.1007/s10822-014-9713-7.
URL http://link.springer.com/10.1007/s10822-014-9713-7

[36] H. Heinz, R. A. Vaia, B. L. Farmer, R. R. Naik, Accurate Simulation of Surfaces and Interfaces of Face-Centered Cubic Metals Using 126 and 96 Lennard-Jones Potentials, The Journal of Physical Chemistry C 112 (44) (2008) 17281–17290. doi:10.1021/jp801931d.
URL http://pubs.acs.org/doi/abs/10.1021/jp801931d

[37] H. Heinz, Adsorption of biomolecules and polymers on silicates, glasses, and oxides: mechanisms, predictions, and opportunities by molecular simulation, Current Opinion in Chemical Engineering 11 (2016) 34–41. doi:10.1016/j.coche.2015.12.003.
URL http://dx.doi.org/10.1016/j.coche.2015.12.003

[38] H. Heinz, B. L. Farmer, R. B. Pandey, J. M. Slocik, S. S. Patnaik, R. Pachter, R. R. Naik, Nature of Molecular Interactions of Peptides with Gold, Palladium, and PdAu Bimetal Surfaces in Aqueous Solution, Journal of the American Chemical Society 131 (28) (2009) 9704–9714. doi:10.1021/ja900531f.
URL http://pubs.acs.org/doi/abs/10.1021/ja900531f

[39] E. Herrero, L. J. Buller, H. D. Abruña, Underpotential Deposition at Single Crystal Surfaces of Au, Pt, Ag and Other Materials, Chemical Reviews 101 (7) (2001) 1897–1930. doi:10.1021/CR9600363.
URL http://dx.doi.org/10.1021/CR9600363

[40] T. Hachiya, H. Honbo, K. Itaya, Detailed underpotential deposition

of copper on gold(III) in aqueous solutions, Journal of Electroanalytical Chemistry and Interfacial Electrochemistry 315 (1) (1991) 275–291. doi:10.1016/0022-0728(91)80076-3.

URL http://dx.doi.org/10.1016/0022-0728(91)80076-3

[41] G. Gunawardena, G. Hills, I. Montenegro, Electrochemical nucleation: Part IV. Electrodeposition of copper onto vitreous carbon, Journal of Electroanalytical Chemistry and Interfacial Electrochemistry 184 (2) (1985) 357–369. doi:10.1016/0368-1874(85)85539-8.

URL http://dx.doi.org/10.1016/0368-1874(85)85539-8

[42] H. Matsumoto, J. Inukai, M. Ito, Structures of copper and halides on Pt(111), Pt(100) and Au(111) electrode surfaces studied by in-situ scanning tunneling microscopy, Journal of Electroanalytical Chemistry 379 (1-2) (1994) 223–231. doi:10.1016/0022-0728(94)87142-6.

URL http://dx.doi.org/10.1016/0022-0728(94)87142-6

[43] C. Prestipino, L. Regli, J. G. Vitillo, F. C. Bonino, A. A. Damin, C. Lamberti, A. Zecchina, P. L. Solari, K. O. Kongshaug, S. Bordiga, Local structure of framework Cu(II) in HKUST-1 metallorganic framework: Spectroscopic characterization upon activation and interaction with adsorbates, Chemistry of Materials 18 (5) (2006) 1337–1346. doi:10.1021/cm052191g.

URL http://dx.doi.org/10.1021/cm052191g

[44] B. Han, Z. Li, T. Wandlowski, Adsorption and self-assembly of aromatic carboxylic acids on Au/electrolyte interfaces., Analytical and bioanalyt-

ical chemistry 388 (1) (2007) 121–129. doi:10.1007/s00216-007-1166-6.
URL http://www.ncbi.nlm.nih.gov/pubmed/17318516

[45] A. Dmitriev, N. Lin, J. Weckesser, J. V. Barth, K. Kern, Supramolecular
Assemblies of Trimesic Acid on a Cu(100) Surface, The Journal of Physical Chemistry B 106 (27) (2002) 6907–6912. doi:10.1021/JP014214U.
URL http://dx.doi.org/10.1021/JP014214U

[46] H. K. Kim, W. S. Yun, M.-B. Kim, J. Y. Kim, Y.-S. Bae, J. Lee, N. C.
Jeong, A Chemical Route to Activation of Open Metal Sites in the
Copper-Based Metal-Organic Framework Materials HKUST-1 and Cu-
MOF-2., Journal of the American Chemical Society 137 (31) (2015)
10009–10015. doi:10.1021/jacs.5b06637.
URL http://dx.doi.org/10.1021/jacs.5b06637

[47] P. Schäfer, M. A. van der Veen, K. F. Domke, Unraveling a two-step
oxidation mechanism in electrochemical Cu-MOF synthesis, Chemical
Communications 52 (25) (2016) 4722–4725. doi:10.1039/C6CC00534A.
URL http://xlink.rsc.org/?DOI=C6CC00534A

[48] U. Mueller, H. Puetter, M. Hesse, M. Schubert, H. Wessel, J. Huff,
M. Guzmann, Method for electrochemical production of a crystalline
porous metal organic skeleton material (2004).
URL http://patents.com/us-7968739.html